

# Supplementary Materials

## Incremental Learning via Robust Parameter Posterior Fusion

Anonymous Authors

### ABSTRACT

In the main manuscript, we propose a Robust Parameter Posterior Fusion ( $\text{RP}^2\text{F}$ ) framework, a novel approach for incremental learning that demonstrates promising performance. This supplementary appendix serves to enrich the description by providing supplementary analysis and details. Section 1 presents the pseudo code elucidating the operations of  $\text{RP}^2\text{F}$ . Section 2 provides the mathematical proof of the MAP estimation in Eq. (10) described in the manuscript. Section 3 conducts empirical analyses to validate the Class-II ability of  $\text{RP}^2\text{F}$ . Section 4 explores the robustness of  $\text{RP}^2\text{F}$  in the task order. Finally, Section 5 offers some details for carrying out experiments.

### 1 PSEUDO CODE

The training of the  $\text{RP}^2\text{F}$  framework for task  $t$  involves a four-stage loop: 1) training the feature extractor  $\theta_t$ ; 2) estimating the Hessian  $\Lambda_t$  surrounding  $\theta_t$ ; 3) updating the fused posterior extractor  $\theta_{1:t}$ ; 4) training the task-specific classifier  $\tau_t$ . Within each task, the four-step iteration **repeats** multiple times until the model converges. We outline the training process of  $\text{RP}^2\text{F}$  in Algorithm 1.

---

#### Algorithm 1: $\text{RP}^2\text{F}$ Training

---

```

Input: Datasets  $\{D_1, \dots, D_T\}$ 
Output: Extractor  $\theta_{1:T}$ ; Classifiers  $\{\tau_1, \dots, \tau_T\}$ 

1 // Learning Task 1.
2 Initialize  $\theta_1, \tau_1$ 
3 for epoch_id = {1, ..., n_epochs} do
4   // Refer to Eq. (19)
5    $\theta_1, \tau_1 \leftarrow$ 
6    $\theta_1, \tau_1 - \alpha \nabla_{\theta_1, \tau_1} L_{ce}(\tau_1 \circ \theta_1, D_1) + \lambda L_{robust\_pri}(\tau_1 \circ \theta_1)$ 
7    $\theta_{1:1} \leftarrow \theta_1$ 
8    $\Lambda_{1:1} \leftarrow \frac{\partial L_{ce}(\theta_1^* + \delta, D_1)}{\eta \partial \delta}$ 
9 // Learning Task 2, ..., T
10 for t = {2, ..., T} do
11    $\theta_t \leftarrow \theta_{t-1}$ 
12   Initialize  $\tau_t$ 
13   for epoch_id = {1, ..., n_epochs} do
14     // Refer to Eq. (20)
15      $\theta_t \leftarrow \theta_t - \alpha \nabla_{\theta_t} L_{ce}(\tau_t \circ \theta_t, D_t) + \lambda L_{robust\_pri}(\tau_t \circ \theta_t)$ 
16      $\Lambda_t \leftarrow \frac{\partial L_{ce}(\theta_t^* + \delta, D_t)}{\eta \partial \delta}$ 
17      $\theta_{1:t} \leftarrow \frac{\Lambda_{1:t-1} \theta_{1:t-1} + \Lambda_t \theta_t}{\Lambda_{1:t-1} + \Lambda_t}$ 
18      $\tau_t \leftarrow \tau_t - \alpha \nabla_{\tau_t} L_{ce}(\tau_t \circ \theta_{1:t}, D_t)$ 
19    $\Lambda_{1:t} \leftarrow \Lambda_{1:t-1} + \Lambda_t$ 
20 return  $\theta_{1:T}, \{\tau_1, \dots, \tau_T\}$ 

```

---

### 2 DETAILS ABOUT MAP ESTIMATION IN EQ. (10)

In the manuscript, Eq. (10) is dedicated to identify the optimal parameter  $\theta_{1:t}^*$  that maximizes the posterior probability  $P(\theta|D_1, \dots, D_t)$ . This maximization process leverages the computational framework established in Eq. (8), where the posterior probability is expressed as a product of prior probabilities and likelihood functions corresponding to each task:

$$\begin{aligned} \theta_{1:t}^* &= \arg \max_{\theta} P(\theta|D_1, \dots, D_t) \\ &= \arg \max_{\theta} \prod_{t'=1}^t P(\theta)^{\frac{1}{t}} P(D_{t'}|\theta). \end{aligned} \quad (1)$$

Employing the Laplace approximation, we estimate  $P(\theta)^{\frac{1}{t}} P(D_{t'}|\theta)$  using a Gaussian distribution  $N(\theta|\theta_{t'}^*, H_t^{*-1})$ . Consequently, the formulation for deriving  $\theta_{1:t}^*$  becomes:

$$\begin{aligned} \theta_{1:t}^* &\approx \arg \max_{\theta} \prod_{t'=1}^t \frac{\sqrt{\det(\Lambda_{t'}^*)}}{(2\pi)^{k/2}} \exp\left(-\frac{1}{2}(\theta - \theta_{t'}^*)^\top \Lambda_{t'}^* (\theta - \theta_{t'}^*)\right) \\ &= \arg \max_{\theta} \log\left(\prod_{t'=1}^t \frac{\sqrt{\det(\Lambda_{t'}^*)}}{(2\pi)^{k/2}} \exp\left(-\frac{1}{2}(\theta - \theta_{t'}^*)^\top \Lambda_{t'}^* (\theta - \theta_{t'}^*)\right)\right) \\ &= \arg \max_{\theta} \sum_{t'=1}^t \left[ \log\left(\frac{\sqrt{\det(\Lambda_{t'}^*)}}{(2\pi)^{\frac{k}{2}}}\right) - \frac{1}{2}(\theta - \theta_{t'}^*)^\top \Lambda_{t'}^* (\theta - \theta_{t'}^*) \right] \\ &= \arg \max_{\theta} \sum_{t'=1}^t \left[ -\frac{1}{2}\theta^\top \Lambda_{t'}^* \theta + \theta^\top \Lambda_{t'}^* \theta_{t'}^* - \frac{1}{2}(\theta_{t'}^*)^\top \Lambda_{t'}^* \theta_{t'}^* \right], \end{aligned} \quad (2)$$

where  $k$  denotes the number of dimensions of  $\theta$ .

By taking the derivative of Equation 2 with respect to the parameter vector  $\theta$ , we obtain the MAP estimation for  $\theta$ :

$$\begin{aligned} \frac{d}{d\theta} \left( \sum_{t'=1}^t \left[ -\frac{1}{2}\theta^\top \Lambda_{t'}^* \theta + \theta^\top \Lambda_{t'}^* \theta_{t'}^* \right] \right) &= 0 \\ \sum_{t'=1}^t [-\Lambda_{t'}^* \theta + \Lambda_{t'}^* \theta_{t'}^*] &= 0 \\ \left( \sum_{t'=1}^t \Lambda_{t'}^* \right) \theta &= \sum_{t'=1}^t \Lambda_{t'}^* \theta_{t'}^* \\ \theta &= \frac{\sum_{t'=1}^t \Lambda_{t'}^* \theta_{t'}^*}{\sum_{t'=1}^t \Lambda_{t'}^*}. \end{aligned} \quad (3)$$

Finally, the expression for  $\theta$  as the weighted average of  $\theta_{t'}^*$ , weighted by their respective precisions  $\Lambda_{t'}^*$ , is taken as the optimal

**Table 1:** Class incremental learning results (ACC %) on 10-split CIFAR-100 and 10-split Tiny-ImageNet. We report the average accuracy (%) and the corresponding standard deviation over five runs with random seeds, and the higher the better. (\*) indicates the upper-bound model that is jointly trained with all tasks. (†) imply the results are quoted from the origin paper or [20], in which the standard deviations may not be provided (HCR, NPCL, and VDFD).

Methods	Venue	Buffer	10-split CIFAR-100	10-split Tiny-ImageNet
Joint*	-	-	70.31	58.07
DER [2]	NeurIPS2020	500	34.24±1.4	17.75±1.1
DER++ [2]	NeurIPS2020	500	36.52±2.0	19.38±1.4
HCR† [22]	KBS2022	500	33.71	22.05
NPCL† [3]	NeurIPS2023	500	37.43	15.29±1.0
Refresh(DER++)† [24]	ICLR2024	500	38.49±0.8	20.81±1.3
FNO(DER++)† [4]	ICLR2024	500	40.81±0.7	22.45±0.4
OWM [26]	NMI2019	-	27.63±0.5	15.30±0.3
DI [25]	CVPR2020	-	11.19±0.3	8.19±0.2
ILCOC [19]	CVPRW2021	-	22.19±1.6	15.78±0.4
EFT [21]	CVPR2021	-	35.99±1.0	26.89±0.6
PASS [29]	CVPR2021	-	31.80±0.7	28.48±0.6
ABD [15]	ICCV2021	-	33.30±0.3	15.80±0.4
FAS [11]	ICLR2022	-	25.79±0.7	24.29±0.3
SSRE† [30]	CVPR2022	-	30.40±0.7	22.93±1.0
DCPOC [18]	PR2023	-	25.80±0.4	19.75±0.1
VDFD† [7]	PAMI2023	-	38.38	26.21
ANCL† [5]	CVPR2023	-	29.77±1.1	22.58±0.8
TA† [20]	WACV2024	-	34.17±0.3	24.78±0.9
MIND [1]	AAAI2024	-	33.52±0.4	26.46±0.1
<b>RP<sup>2</sup>F(Ours)</b>	-	-	<b>42.33±0.7</b>	<b>28.82±0.3</b>

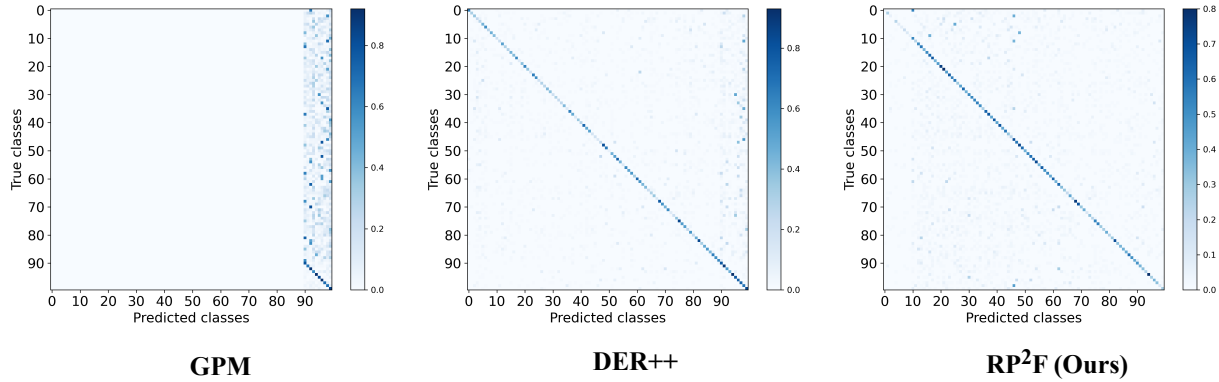


**Figure 1: Confusion matrix of DER++, GPM, and RP<sup>2</sup>F on 10-Split CIFAR-100.**

value of  $\theta_{1:t}^*$ :

$$\theta_{1:t}^* \approx \frac{\sum_{t'=1}^t \Lambda_{t'}^* \theta_{t'}^*}{\sum_{t'=1}^t \Lambda_{t'}^*}. \quad (4)$$

### 3 CLASS-IL ABILITY ANALYSIS

Different from Task-II, Class Incremental Learning (Class-IL) [28] does not provide task identification during inference, and also garnered significant attention from the research community. Although Class-IL is not the primary focus of this study, we observe that our RP<sup>2</sup>F model is applicable to Class-IL, even under the more challenging conditions of the exemplar-free restriction [10].

Table 2: Hyperparameters for some baseline models and our RP<sup>2</sup>F. In this context, "KD" stands for "Knowledge Distillation"

Methods	Hyperparameters
LwF [8]	learning rate: 0.01 batch size: 32 temperature: 2 KD weight: 5e-4
SI [27]	learning rate: 0.1 (CIFAR-100), 0.05 (Tiny-ImageNet) batch size: 16 regularizer weight: 0.5
GEM [9]	learning rate: 0.03 (CIFAR-100), 0.05 (Tiny-ImageNet) batch size: 32 (CIFAR-100), 64 (Tiny-ImageNet)
DER [2]	learning rate: 0.03 batch size: 32 KD weight: 0.1
DER++ [2]	learning rate: 0.03 batch size: 32 KD weight $\alpha$ : 0.1 $\beta$ : 0.5
EFT [21]	learning rate: 0.005 (CIFAR-100), 0.002 (Tiny-ImageNet) batch size: 64 (CIFAR-100), 16 (Tiny-ImageNet)
PASS [29]	learning rate: 1e-4 (Tiny-ImageNet), 5e-4 (CIFAR-100) batch size: 64 (CIFAR-100), 32 (Tiny-ImageNet) KD weight: 10 (Tiny-ImageNet), 0.2 (CIFAR-100) prototype weight: 0.05 (CIFAR-100), 0.5 (Tiny-ImageNet)
GPM [12]	learning rate: 0.02 (CIFAR-10), 0.01 (CIFAR-100), 0.02 (Tiny-ImageNet) batch size: 64 (CIFAR-10, CIFAR-100), 32 (Tiny-ImageNet)
Adam-NSCL [23]	learning rate: 1e-5 (CIFAR-10), 1e-4 (CIFAR-100), 5e-5 (Tiny-ImageNet) batch size: 32 (CIFAR-10, CIFAR-100), 16 (Tiny-ImageNet)
FAS [11]	learning rate: 0.001 (CIFAR-100), 5e-4 (Tiny-ImageNet) batch size: 32 (CIFAR-100), 16 (Tiny-ImageNet)
DCPOC [18]	learning rate: 5e-5 batch size: 8 (CIFAR-100), 32 (Tiny-ImageNet) $\lambda_1$ : 20 (CIFAR-100), 10 (Tiny-ImageNet) $\lambda_2$ : 10 (CIFAR-100), 0.01 (Tiny-ImageNet)
PRAKA [13]	learning rate: 0.001 batch size: 64 (CIFAR-100), 128 (Tiny-ImageNet) temperature: 0.1 (CIFAR-100), 0.2 (Tiny-ImageNet) KD weight: 20 (CIFAR-100), 15 (Tiny-ImageNet)
MIND [1]	learning rate: 0.005 (CIFAR-100), 0.002 (Tiny-ImageNet) batch size: 256 temperature: 6.5 (CIFAR-100), 12 (Tiny-ImageNet)
RP <sup>2</sup> F (ours)	learning rate: 0.05 (CIFAR-100), 0.3 (Tiny-ImageNet) batch size: 32 (CIFAR-100), 1024 (Tiny-ImageNet) parameter-robustness regularizer weight $\lambda$ : 1e-5

During the inference phase for Class-IL, for a given sample  $x$  without task identification, we concatenate all task-specific classifiers into a unified one  $\tau^* = [\tau_1^* \dots \tau_T^*]$  to perform the prediction as follows:

$$\hat{y} = f(x; \tau^* \circ \theta_{1:T}^*). \quad (5)$$

To evaluate the Class-IL performance of the RP<sup>2</sup>F model, we compare it against several established Class-IL baselines, including DER [2], DER++ [2], HCR [22], NPCL [3], Refresh [24], FNO [4], OWM [26], DI [25], ILCOC [19], EFT [21], PASS [29], ABD [15], FAC [11], SSRE [30], DCPOC [18], VDFD [7], ANCL [5], TA [20], and MIND [1]. For exemplar-based methods, we provide them with an additional buffer that can store up to 500 samples. The results on 10-split CIFAR-100 and 10-split Tiny-ImageNet are presented in Table 1. As can be seen, our work also demonstrates competitive performance in the Class-IL setting. For the 10-split CIFAR-100, we achieve a classification accuracy of 42.33%, with a margin of 1.52%

over the second-best method. Similarly, as for the more challenging 10-split Tiny-ImageNet dataset, our work is 0.34% more accurate than the second-best method. All these results confirm the superior performance of RP<sup>2</sup>F in the Class-IL setting.

We further evaluate the Class-IL performance of RP<sup>2</sup>F under various lengths of task sequences. Following [15], we conduct experiments on CIFAR-100 with 5, 10, and 20 tasks. The comparison involved several methods including DGR [14], LWF [8], DI [25], ABD [15], PASS [29], DCPOC [18], and DLCPA [17], with their respective performances detailed in Table 3. RP<sup>2</sup>F outperformed all other methods in each setting, surpassing the second-best method by margins of 3.7%, 2.2%, and 3.8%, respectively. These results validate the robustness of RP<sup>2</sup>F for the length of the task sequence.

Additionally, we compute the confusion matrices of DER++, GPM, and RP<sup>2</sup>F, to analysis the balance of classifications in Class-IL. As illustrated in Figure 1, the classification of GPM tends to

349  
350  
**Table 3: Class incremental learning results (ACC %) on CIFAR-100 for various task numbers (5, 10, 20).**

Task Number	5 tasks	10 tasks	20 tasks
DGR[14]	14.4	8.1	4.1
LwF[8]	17.0	9.2	4.7
DI[25]	18.8	10.9	5.7
ABD[15]	43.9	33.7	20.0
PASS[29]	45.2	30.8	17.4
DCPOC[18]	33.1	27.5	20.5
DLCPA[17]	46.3	40.1	26.4
RP <sup>2</sup> F (Ours)	<b>50.0</b>	<b>42.3</b>	<b>30.2</b>

362 the classes of the last task. This phenomenon is expected, as GPM  
363 is designed for Task-IL and lacks a specific design to counteract  
364 classification bias. For DER++, the phenomenon of classification  
365 bias is significantly reduced, thanks to the stored old-task exemplars.  
366 Significantly, the confusion matrix for RP<sup>2</sup>F displays pronounced  
367 diagonal concentration, indicating a robust balance in classification  
368 across tasks. This result underscores the effectiveness of RP<sup>2</sup>F in  
369 achieving equitable performance across all classes in the Class-IL  
370 setting.

372  
373 **Table 4: Incremental learning result (ACC %) of RP<sup>2</sup>F on a  
374 10-split CIFAR-100 with five random task orders.**

Methods	CIFAR-100	
	Class-IL	Task-IL
Task order 1	42.73	83.07
Task order 2	42.01	82.83
Task order 3	43.29	83.34
Task order 4	42.04	83.07
Task order 5	42.19	82.62
Average	42.45±0.49	82.99±0.24

## 4 ROBUSTNESS ANALYSIS ON TASK ORDER

386 This subsection investigates the robustness of RP<sup>2</sup>F to the task  
387 order. We randomly shuffle the task order on CIFAR-100 and retrain  
388 RP<sup>2</sup>F incrementally five times. Table 4 presents the results for each  
389 order and the average performance. As observed, RP<sup>2</sup>F exhibits  
390 relatively stable performance across different scenarios, indicating  
391 its robustness to task orders.

393  
394 **Table 5: Dataset statistics.**

Dataset	CIFAR-100	Tiny-ImageNet
Input size	$3 \times 32 \times 32$	$3 \times 64 \times 64$
# Classes	100	200
# Training samples per class	450	450
# Validation samples per class	50	50
# Testing samples per class	100	100

## 5 EXPERIMENTAL DETAILS

404 This section provides details of the experimental setup. All experiments  
405 detailed in our manuscript and appendix were conducted on

406 a workstation running Ubuntu 16.04, equipped with 18 Intel Xeon  
407 2.60GHz CPUs, 256 GB of memory, and 6 NVIDIA RTX3090 GPUs.  
408 Python 3.8 was used to implement all the methods.

409 Hyperparameters tuned for both the baseline methods, which  
410 were implemented by ourselves, and the proposed RP<sup>2</sup>F are sum-  
411 marized in Table 2. Additionally, statistical details of the datasets  
412 (CIFAR-100 [6] and Tiny-ImageNet [16]) are provided in Table 5.

## REFERENCES

- [1] Jacopo Bonato, Francesco Pelosin, Luigi Sabetta, and Alessandro Nicolosi. 2024. MIND: Multi-task incremental network distillation. (2024).
- [2] Pietro Buzzega, Matteo Boschini, Angelo Porrello, Davide Abati, and SIMONE CALDERARA. 2020. Dark experience for general continual learning: A strong, simple baseline. In *Advances in Neural Information Processing Systems*, Vol. 33. 15920–15930.
- [3] Saurav Jha, Dong Gong, He Zhao, and Lina Yao. 2023. NPCL: Neural processes for uncertainty-aware continual learning. In *Advances in Neural Information Processing Systems*.
- [4] Hoyong Kim and Kangil Kim. 2024. Fixed non-negative orthogonal classifier: Inducing zero-mean neural collapse with feature dimension separation. In *International Conference on Learning Representations*.
- [5] Sanghwan Kim, Lorenzo Noci, Antonio Orvieto, and Thomas Hofmann. 2023. Achieving a better stability-plasticity trade-Off via auxiliary networks in continual learning. In *IEEE Conference on Computer Vision and Pattern Recognition*. 11930–11939.
- [6] Alex Krizhevsky. 2012. Learning multiple layers of features from tiny images. *University of Toronto* (05 2012).
- [7] Xiaorong Li, Shipeng Wang, Jian Sun, and Zongben Xu. 2023. Variational data-free knowledge distillation for continual learning. *IEEE Transactions on Pattern Analysis and Machine Intelligence* 45, 10 (2023), 1–17.
- [8] Zhizhong Li and Derek Hoiem. 2017. Learning without forgetting. *IEEE Transactions on Pattern Analysis and Machine Intelligence* 40, 12 (2017), 2935–2947.
- [9] David Lopez-Paz and Marc' Aurelio Ranzato. 2017. Gradient episodic memory for continual learning. In *Advances in Neural Information Processing Systems*, Vol. 30. 6467–6476.
- [10] Marc Masana, Xialei Liu, Bartłomiej Twardowski, Mikel Menta, Andrew D. Bagdanov, and Joost van de Weijer. 2022. Class-incremental learning: survey and performance evaluation on image classification. *IEEE Transactions on Pattern Analysis and Machine Intelligence* (2022), 1–20.
- [11] Zichen Miao, Ze Wang, Wei Chen, and Qiang Qiu. 2022. Continual learning with filter atom swapping. In *International Conference on Learning Representations*.
- [12] Gobinda Saha, Ishu Garg, and Kaushik Roy. 2021. Gradient projection memory for continual learning. In *International Conference on Learning Representations*.
- [13] Wuxuan Shi and Mang Ye. 2023. Prototype reminiscence and augmented asymmetric knowledge aggregation for non-exemplar class-incremental learning. In *IEEE International Conference on Computer Vision*. 1772–1781.
- [14] Hanul Shin, Jung Kwon Lee, Jaehong Kim, and Jiwon Kim. 2017. Continual learning with deep generative replay. In *Advances in Neural Information Processing Systems*, Vol. 30.
- [15] James Smith, Yen-Chang Hsu, Jonathan Balloch, Yilin Shen, Hongxia Jin, and Zsolt Kira. 2021. Always be dreaming: A new approach for data-free class-incremental learning. In *IEEE International Conference on Computer Vision*.
- [16] Stanford. 2015. Tiny imageNet challenge (CS231n). <http://tiny-imagenet.herokuapp.com/>. (2015). <http://tiny-imagenet.herokuapp.com/>
- [17] Wenju Sun, Qingyong Li, Wen Wang, and Yangli-ao Geng. 2023. Towards plastic and stable exemplar-free incremental learning: A dual-learner framework with cumulative parameter averaging. *arXiv preprint arXiv:2310.18639* (2023).
- [18] Wenju Sun, Qingyong Li, Jing Zhang, Danyu Wang, Wen Wang, and YangLi ao Geng. 2023. Exemplar-free class incremental learning via discriminative and comparable parallel one-class classifiers. *Pattern Recognition* 140 (2023), 109561.
- [19] Wenju Sun, Jing Zhang, Danyu Wang, Yangli-ao Geng, and Qingyong Li. 2021. ILLOC: An incremental learning framework based on contrastive one-class classifiers. In *IEEE Conference on Computer Vision and Pattern Recognition Workshops*. 3580–3588.
- [20] Filip Szatkowski, Mateusz Pyla, Marcin Przewięźlikowski, Sebastian Cygert, Bartłomiej Twardowski, and Tomasz Trzcinski. 2024. Adapt your teacher: Improving knowledge distillation for exemplar-free continual learning. In *IEEE Winter Conference on Applications of Computer Vision*. 1977–1987.
- [21] Vinay Kumar Verma, Kevin J Liang, Nikhil Mehta, Piyush Rai, and Lawrence Carin. 2021. Efficient feature transformations for discriminative and generative continual learning. In *IEEE Conference on Computer Vision and Pattern Recognition*. 13865–13875.
- [22] Qiang Wang, Jiayi Liu, Zhong Ji, Yanwei Pang, and Zhongfei Zhang. 2022. Hierarchical correlations replay for continual learning. *Knowledge-Based Systems* 250 (2022), 105–116.

- (2022), 109052.

[23] Shipeng Wang, Xiaorong Li, Jian Sun, and Zongben Xu. 2021. Training networks in null space of feature covariance for continual learning. In *IEEE Conference on Computer Vision and Pattern Recognition*. 184–193.

[24] Zhenyi Wang, Yan Li, Li Shen, and Heng Huang. 2024. A unified and general framework for continual learning. In *International Conference on Learning Representations*.

[25] Hongxu Yin, Pavlo Molchanov, Jose M. Alvarez, Zhizhong Li, Arun Mallya, Derek Hoiem, Niraj K. Jha, and Jan Kautz. 2020. Dreaming to distill: data-free knowledge transfer via deepinversion. In *IEEE Conference on Computer Vision and Pattern Recognition*.

[26] Guanxiang Zeng, Yang Chen, Bo Cui, and Shan Yu. 2019. Continual learning of context-dependent processing in neural networks. *Nature Machine Intelligence* 1, 8 (2019), 364–372.

[27] Friedemann Zenke, Ben Poole, and Surya Ganguli. 2017. Continual learning through synaptic intelligence. In *International Conference on Machine Learning*. 3987–3995.

[28] Da-Wei Zhou, Qi-Wei Wang, Zhi-Hong Qi, Han-Jia Ye, De-Chuan Zhan, and Ziwei Liu. 2023. Deep class-incremental learning: a survey. *arXiv preprint arXiv:2302.03648* (2023).

[29] Fei Zhu, Xu-Yao Zhang, Chuang Wang, Fei Yin, and Cheng-Lin Liu. 2021. Prototype augmentation and self-supervision for incremental learning. In *IEEE Conference on Computer Vision and Pattern Recognition*. 5871–5880.

[30] Kai Zhu, Wei Zhai, Yang Cao, Jiebo Luo, and Zheng-Jun Zha. 2022. Self-sustaining representation expansion for non-exemplar class-incremental learning. In *IEEE Conference on Computer Vision and Pattern Recognition*. 9296–9305.